Evaluation of the magnetization direction effects on ferrite PM brushless fractional machines

AIP Journal of Applied Physics

Broadband light sources based on InAs/InGaAs metamorphic quantum dots

L. Seravalli, M. Gioannini, F. Cappelluti, F. Sacconi, G. Trevisi, and P. Frigeri

Citation: Journal of Applied Physics **119**, 143102 (2016); doi: 10.1063/1.4945436
View online: http://dx.doi.org/10.1063/1.4945436
View Table of Contents: http://scitation.aip.org/content/aip/journal/jap/119/14?ver=pdfcov
Published by the AIP Publishing

Broadband light sources based on InAs/InGaAs metamorphic quantum dots

L. Seravalli,[1] M. Gioannini,[2] F. Cappelluti,[2] F. Sacconi,[3] G. Trevisi,[1] and P. Frigeri[1]
[1]*CNR-IMEM, Parco delle Scienze 37a, I-43100 Parma, Italy*
[2]*Politecnico di Torino, DET - C.so Duca degli Abruzzi 24, I-10129 Torino, Italy*
[3]*Tiberlab Srl, Via del Politecnico, 1-00133 Roma, Italy*

(Received 18 January 2016; accepted 24 March 2016; published online 8 April 2016)

We propose a design for a semiconductor structure emitting broadband light in the infrared, based on InAs quantum dots (QDs) embedded into a metamorphic step-graded $In_xGa_{1-x}As$ buffer. We developed a model to calculate the metamorphic QD energy levels based on the realistic QD parameters and on the strain-dependent material properties; we validated the results of simulations by comparison with the experimental values. On this basis, we designed a p-i-n heterostructure with a graded index profile toward the realization of an electrically pumped guided wave device. This has been done by adding layers where QDs are embedded in $In_xAl_yGa_{1-x-y}As$ layers, to obtain a symmetric structure from a band profile point of view. To assess the room temperature electroluminescence emission spectrum under realistic electrical injection conditions, we performed device-level simulations based on a coupled drift-diffusion and QD rate equation model. On the basis of the device simulation results, we conclude that the present proposal is a viable option to realize broadband light-emitting devices. © *2016 AIP Publishing LLC*.
[http://dx.doi.org/10.1063/1.4945436]

I. INTRODUCTION

Recently, there is an increasing interest in the use of InAs quantum dots (QDs) for broadband light sources in the infrared: superluminescent diodes (SLDs) based on QDs have been fabricated for medical applications such as Optical Coherence Tomography (OCT).[1–4] To increase the spectral bandwidth, it is necessary to engineer the energy levels of QDs.[1] One of the most successful methods involves the use of InGaAs capping layer that causes a reduction of band discontinuities and QD strain; this has allowed to redshift the emission of QDs in the 1.3 μm range at room temperature (RT) and to increase the emission bandwidth up to 170 nm.[5,6] Chirped dot-in-a-well structure was also proposed to achieve broadband emission[7,8] by tailoring the composition of the InGaAs quantum well (QW) or the thickness of the cap layer; broad optical spectra at 1.55 μm were achieved with quantum dashes exploiting both the ground state (GS) and excited state (ES) emission.[9] InAs QDs deposited on InGaAs metamorphic buffers (MBs), i.e., metamorphic QDs, are very interesting structures. Indeed, this approach has been demonstrated as very successful in shifting the light emission of InAs QDs to 1.3 μm and 1.55 μm and even beyond this value;[10–13] recently, such nanostructures have been demonstrated as effective single photon sources in the telecom range.[14–16] In addition, devices based on metamorphic QDs have been fabricated with satisfying performances.[17–19] It is hence noteworthy that the presence of structural defects, known to be present in the MB, did not forbid the fabrication of performance devices not limited to light emitting sources: metamorphic solar cells,[20] metamorphic high-mobility transistors,[21,22] and metamorphic optical amplifiers.[23]

In recent years, we have demonstrated that metamorphic QDs are very flexible nanostructures from a design point of view, as they provide several degrees of freedom to control properties of interest:[24] as an example, this allowed to reach RT emission up to 1.59 μm.[13] It is also worth noticing that the QD density in these nanostructures is usually higher than in structures where InAs QDs are deposited over GaAs, reaching values as high as 10^{11} cm^{-2}.[25]

In this work, we propose a RT broadband light source with a large bandwidth based on metamorphic InAs QDs. We study two different structures: structure (A) has QDs inserted into a 4-step graded $In_xGa_{1-x}As$ MB with $x = 0$, 0.10, 0.20, 0.30, 0.40, and it is studied to demonstrate the capability of this approach of tuning the QD emission over a broad spectral range;[26] structure (B) is a symmetric structure (from a band profile point of view) obtained by adding $In_{0.30}Al_yGa_{0.70-y}As$ layers lattice-matched to structure (A) and with Al compositions y selected to give the same energy gaps of $In_xGa_{1-x}As$ layers with $x < 0.30$. To sustain this proposal, we rely on (i) calculations of the confined QD levels, carried out with the TiberCAD software[27,28] using realistic experimental input parameters for nanostructures and materials, and (ii) by using calculated band-structure from (i), we simulate a realistic electrical device operating at RT, where the QD layers are inserted in the intrinsic region of a *p-i-n* heterojunction. The simulator used in part (ii) is a physics-based model coupling drift-diffusion equations for bulk carriers and phenomenological rate equations (REs) for QDs. This model, developed by some of us,[29,30] is a unique tool for the analysis of semiconductor devices with embedded QD layers because it accounts, via QD rate equations, the actual nature of the QD carrier dynamics without making use of the simplified equivalent models of the QD layers. In this way, we can precisely analyse how the de-synchronized[31] electron and hole dynamics in the QDs and the different transport of electrons and holes in the barrier produce a

non-uniform carrier filling of the different QD layers, thus impacting the broadband optical properties. Whereas such an analysis was previously carried on in broadband QW optical devices,[32] this is the first time this study is carried on in p-i-n QD junctions with "chirped" QD layers. In all of these broadband chirped structures, the non-uniform carrier filling of the various chirped layers is indeed relevant issue that significantly limits the broadband performance of the devices.[33]

For the simulations of quantum levels, we calculated the values of strain for each layer of the step-graded InGaAs MB, in order to have reliable input parameters for InAs/InGaAs mismatch values and band discontinuities. The values predicted by the model were validated against the available experimental data, providing a good confidence in the present calculation.

The QD energy levels and structure band profiles for structure (B) are then used to simulate realistic devices operating at RT, where the QD layers are inserted in the intrinsic region of a *p-i-n* heterojunction. Preliminary electroluminescence (EL) spectra were presented in Ref. 26 for a p-i-n device based on structure (A), with GaAs on the bottom p-side and with $In_{0.3}Al_{0.29}Ga_{0.41}As$ on the top n-side, lattice matched to the MB, and with an energy gap equal to GaAs. The analysis carried on in Ref. 26 evidenced that, under realistic electrical injection conditions at room T, transport through the ladder-like bands (typical of structure A) favours QD filling in the lower gap metamorphic layers, thus allowing a rather irregular broadband EL spectrum at RT. In this paper, we improve the design of this structure by further engineering the metamorphic epilayer structure with the aim at realizing a symmetric graded index structure allowing for electrical and optical confinements (structure B).

II. DESIGN OF THE BROADBAND EMISSION METAMORPHIC QD LAYERS

In Figure 1, we show a schematic of the proposed structure (A) where InAs QDs are embedded in the middle of each layer of the 4-step graded InGaAs metamorphic buffer, including a first layer of QDs embedded in GaAs. For this grading profile, we calculated the values of strain on the basis of the model by Romanato *et al.*,[34,35] without taking in consideration the presence of QDs.

The mismatch between the epitaxial layer and the substrate is defined as

$$f = (a_{MB}(t) - a_0)/a_0, \tag{1}$$

where a_0 is the GaAs lattice parameter and $a_{MB}(t)$ is the MB lattice parameter; assuming Vegard's rule, f is proportional to the composition, $f = 0.071\ x$.

We define T as the total thickness of MB of 400 nm and t_0 the thickness of the strain-relaxed region, above which the layer is free of misfit dislocations. We then followed the analysis of Ref. 34, by applying the relation

$$[f(t_0) - f_{eq}]^2 (T - t_0) = K, \tag{2}$$

where f_{eq} is the average mismatch of InGaAs layers at points T and t_0, $f(t_0)$ is the mismatch at t_0 and K a given constant of 3.7×10^{-3} nm for InGaAs material.[35] From (2), we derived the value of $T - t_0$ of 135 nm for the step-graded InGaAs MB.

The strain $\varepsilon = [a_{MB}(x) - a_{free}(x)]/a_{free}(x)$, with $a_{free}(x)$ the free standing lattice parameter of $In_xGa_{1-x}As$, profile in the MB is 0 for $0 < t \leq t_0$ and $[f(t_0) - f(t)]$ for $t_0 < t \leq T$ (Fig. 1, left). This results in having a full strain relaxation in layers with $x = 0.10$, 0.20, and 0.30, while only the last layer with $x = 0.40$ is strained, with $\varepsilon = -0.7\%$. The lattice parameter $a_{MB}(x)$ for each step of the MB can be derived, corresponding to the free standing value for all layers, except for the $x = 0.40$ layer where the value corresponds to a_{MB} ($x = 0.30$).

Once the exact values of x and $a_{MB}(x)$ were derived, they were used as input parameters for the calculation of QD ground levels in each grading step.

For this, we used the multiscale simulation software TiberCAD, already successfully used to simulate the optical properties of semiconductor low-dimensional nanostructures.[36–38] The calculation of strain in lattice mismatched heterostructures is based on the linear elasticity theory of solids[39] by minimizing the elastic energy of the system. This approach is suitable from a computational point of view, and the results can be easily included in a k·p model.

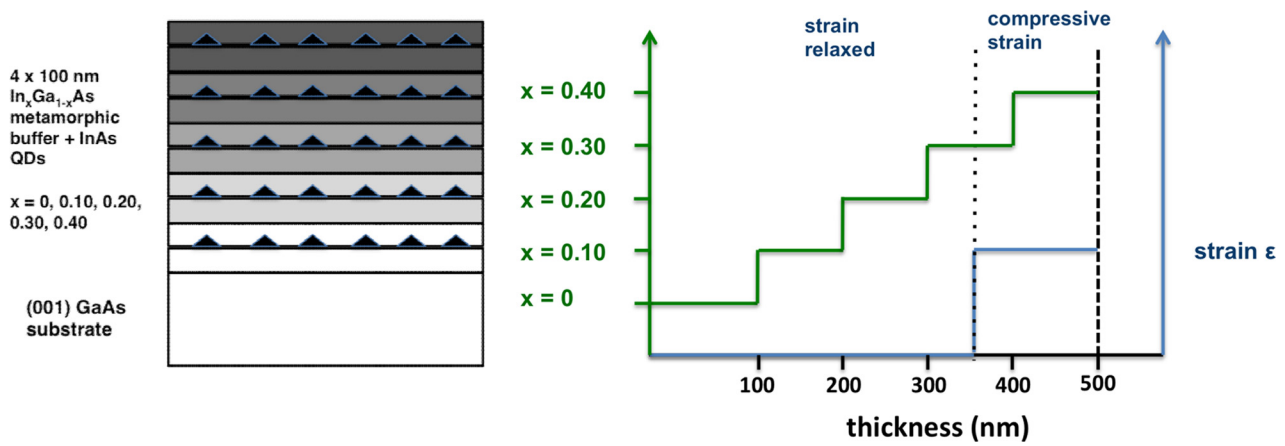

FIG. 1. Schematics of the metamorphic structure (A) (left) and dependence of composition x and strain ε of on the thickness the InGaAs step-graded MB (right). The dotted line indicates the separation between the strain-relaxed and compressed regions (see discussion in the text).

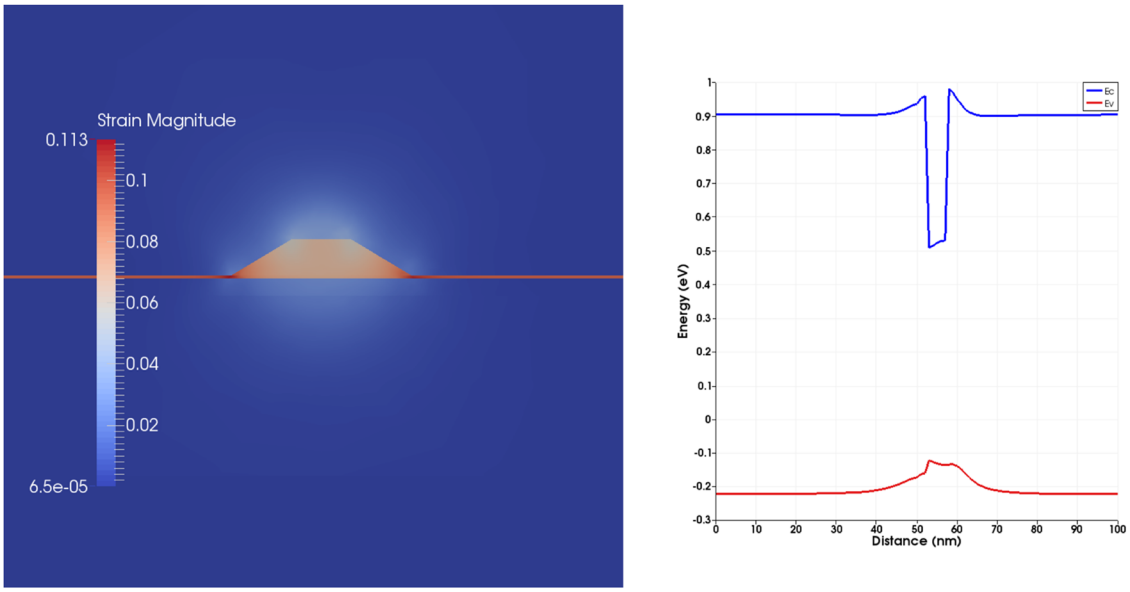

FIG. 2. (Left) Strain map of a simulated InAs QD embedded in $In_{0.20}Ga_{0.80}As$ metamorphic layers. (Right) Band profile for the same structure along the growth direction (vertical axis of left figure).

Quantum mechanical models based on the envelope function approximation (EFA) are used for the calculation of eigenstates of confined particles in QDs, by constructing the Hamiltonian of the system in the framework of the single-band and multiband k·p theory.

The simulated three-dimensional model includes an InAs QD with truncated conical shape, with a ratio of 3 between the base and top diameters: the values were taken from the experimental data available for the InAs QDs grown on the metamorphic InGaAs buffers.[25] The InAs wetting layer (WL) was also taken into consideration, using parameters depending on the $In_xGa_{1-x}As$ metamorphic layer properties.[25,40] Strain calculations have been performed assuming as a substrate material the InGaAs MB layer with the previously derived lattice constants. The strain tensor components of each QD, induced by the mismatch f_{QD} between the QD and the InGaAs MB, defined as

$$f_{QD} = (a_{InAs} - a_{MB}(x))/a_{MB}(x) \tag{3}$$

are obtained and fed in the TiberCAD quantum model. The calculated deformation potentials were applied to InAs bands, while for energy gaps of InGaAs metamorphic layers, we followed the approach of Ref. 40 by taking into consideration the amount of strain as deduced by relations (2) and (1). The Schroedinger equation is then solved by a single-band, effective-mass approach for electrons and a 6 bands k·p approach for holes: the effective mass approximation for electrons is considered satisfying when QD ground states calculation is needed, as in this case.[41] An important parameter is the value $Q_c = \Delta E_c/\Delta E_v$ of band discontinuities between the InAs QDs and InGaAs MBs: for the InAs/GaAs system, $Q_c = 0.80$ is recommended.[42,43] Recently, it has been shown that this value stands also for GaAs/InGaAs heterostructures with the strained InGaAs.[44] The effective mass for electrons depends on the strain; hence, a modified value is necessary for QDs: we followed Refs. 42 and 43 taking a value of 0.022 m_0. All other relevant parameters for the $In_xGa_{1-x}As$ material were taken from Ref. 45, also considering the presence of bowing parameters.

In Figure 2, we show the color map of the strain magnitude and the profile of bands along the growth direction of the metamorphic InAs QDs embedded in a relaxed $In_{0.20}Ga_{0.80}As$ layer. In Figure 3, we show a calculated band profile of the complete structure (A).

For a confident validation of the model, we compared the predicted values of the calculated QD ground state transition energies against experimental peak PL emission energies, also for structures with the InAlAs barriers. In Figure 4, we show a comparison of 10 K PL data, taken from Refs. 12, 13, and 46 and model calculations; a reduction of 20 meV in this latter value was considered to take into consideration the excitonic effects of the experimental emission energies. From Figure 4, the good agreement between the model and

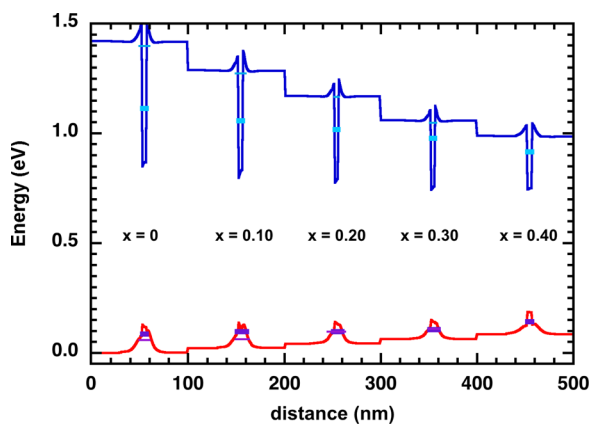

FIG. 3. Conduction (blue) and valence (red) energy bands for structure (A) of Fig. 1 along the growth direction. Calculated energy levels for electrons (cyan) and heavy holes (purple) confined in QDs (squares) and WL (lines) are indicated.

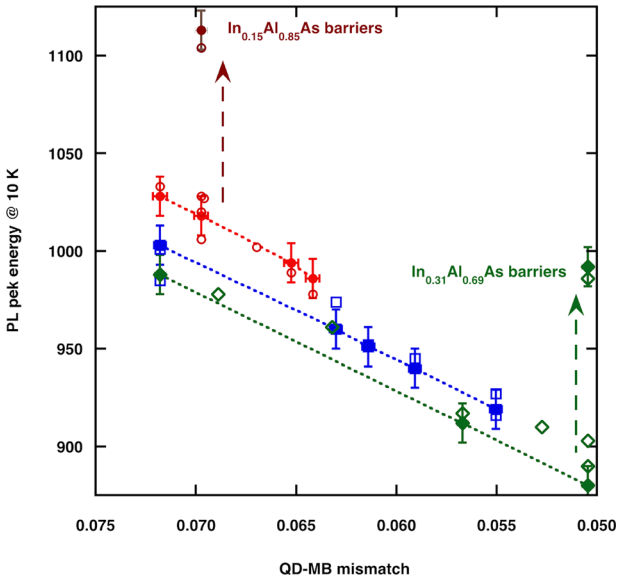

FIG. 4. Experimental (open symbols) and model calculation (filled symbols) of 10 K PL emission of metamorphic InAs/(InAlAs)/$In_xGa_{1-x}As$ QD nanostructures as functions of the QD-MB mismatch for x = 0.15 (circles), x = 0.28 (squares), and x = 0.31 (diamonds). The dashed arrows indicate the effect of InAlAs barriers on emission energies. The dotted lines are guide for the eye. The error bars are calculated considering uncertainties in AFM estimation of QD sizes and calibration of In composition of MB.

experimental values is evident, with discrepancies never larger than 20 meV, a value fully accounted for by the experimental uncertainties in the AFM measurement of QD dimensions and in experimental calibration of *x*, indicated by the error bars.[46,47] It should be stressed that there are no free parameters in this model to be adjusted. The asymmetric band profile shown in Figure 3 (i.e., from a wide to narrow gap) turns to be critical in view of the realization of broadband guided wave light emitters such as a SLDs. For this reason, we have then designed the symmetric structure (B), which can provide broadband emission, and it is also more indicated for the realization of a graded index waveguide.

In Figure 5, we show the structure (B), obtained by adding a second $In_{0.30}Ga_{0.70}As$ layer and three $In_{0.30}Al_yGa_{0.70-y}As$ layers with QDs embedded. The use of InAlGaAs was necessary to have layers lattice-matched to structure (A) that has a lattice parameter a_{MB} (x = 0.30) and with higher energy gaps. The value of y was determined by imposing that each top $In_{0.30}Al_yGa_{0.70-y}As$ layer had the same energy gap of the corresponding bottom $In_xGa_{1-x}As$ layer. Hence, we also performed calculation of the bandstructure and confined QD states on the symmetric structure (B) with results shown in Figure 6.

III. DEVICE-LEVEL SIMULATION OF RT ELECTROLUMINESCENCE OF THE BROADBAND METAMORPHIC QD LAYERS

The proposed multilayer structure (B) was inserted into a realistic *p-i-n* device to prove its capability to produce a broadband emission spectra under electrical pumping at room temperature. In particular, the highly doped p- and n-regions are realized by $Al_{0.26}Ga_{0.74}As$ and $In_{0.30}Al_{0.5}Ga_{0.20}As$, lattice matched to the bottom and top layer of structure (B), respectively.

The device was simulated by exploiting a 1D model that includes a drift-diffusion description of the bulk material (i.e., the metamorphic layers embedding each QD layer) and a set of phenomenological REs for the QD carrier dynamics.[29,30] This allows to study in a rigorous way how, under electrical injection, the QD states are populated, taking into account both their energy distribution and the effect of the transport of electrons and holes, injected from the opposite sides of the junction, through the complex multilayer structure constituting the intrinsic region. The detailed description of the modelling approach is reported in Ref. 29, and we briefly summarize here the most relevant concepts.

The REs for the QD layers include the electron and hole capture from the barriers into the WL state of each layer and the cascade relaxation process in the ES and GS. Since we focus on the modelling at room temperature, the escape from the GS and ES to the higher energy states as well as the escape out of the QD layers to the barrier is governed by the thermal escape. The inter-sub-band electron and hole dynamics in the QD states are modelled by characteristic scattering times (i.e., capture, relaxation time constants). Here, we assume that electrons and holes are captured in/escape out of the QDs independently, with a

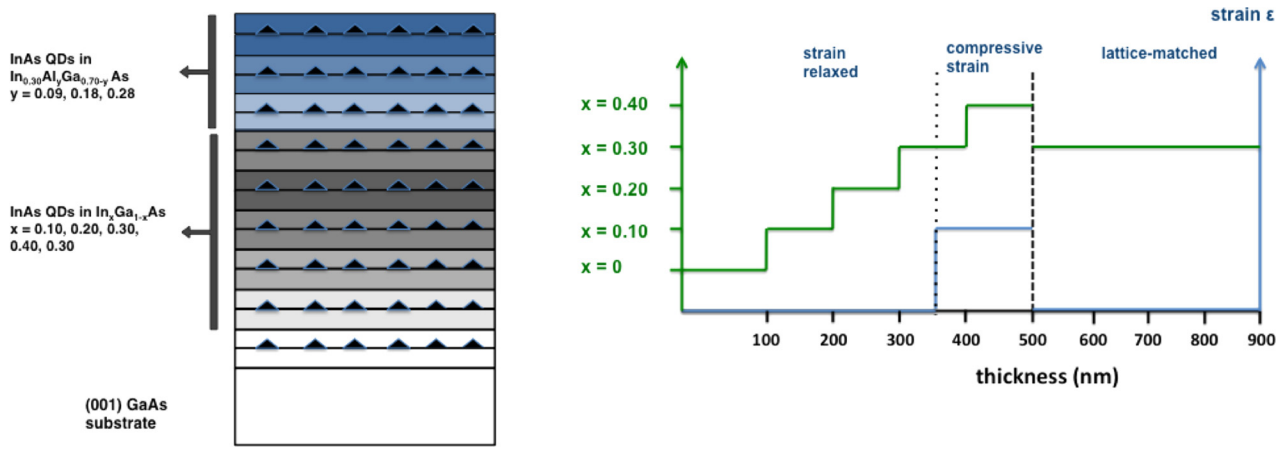

FIG. 5. Schematics of the metamorphic structure (B) (left) and dependence on the thickness of composition x and strain ε (right). The dotted line indicates the separation between the strain-relaxed and compressed regions, and the dashed line indicates separation between the compressed region and lattice-matched layers.

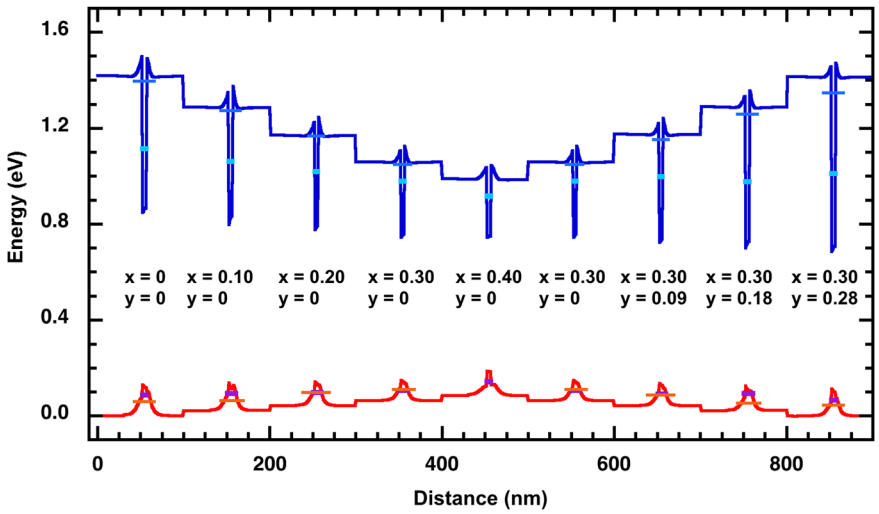

FIG. 6. Conduction (blue) and valence (red) energy bands for structure (B) of Fig. 5 along the growth direction. The values of x and y for each $In_xAl_yGa_{1-x-y}As$ layer are indicated. The calculated energy levels for electrons (cyan) and heavy holes (purple) confined in QDs (squares) and WL (dashed lines) are indicated.

TABLE I. Parameters used for the QD simulations.

QD Parameters	Value
QD density per layer	10^{11} cm^{-2}
Capture and relaxation times for electrons/holes	…
Barrier to WL	0.3 ps/0.1 ps
WL to ES	10 ps/1 ps
ES to GS	2 ps/1 ps
Radiative recombination lifetime for GS, ES, and WL	1 ns

dynamics governed by the carrier-carrier scattering with the electrons or holes accumulated in the WL. This is indeed the dominant mechanism governing the QD carrier dynamics when the QD layers are embedded in a forward biased junction such as in the case of QD lasers and amplifiers.[31] We assume time constants of the order of few picoseconds or hundreds of femtoseconds.[48]

The different electron and hole dynamics can cause a charge imbalance in both the QD layers and in the bulk regions; this imbalance is included in the model since the Poisson equation is self-consistently solved with the bulk drift diffusion equations coupled with the QD rate equations.[29] The potential bending around the central QD layer, for example, is indeed also caused by the excess of holes accumulated in the barrier.

Carrier loss in the QD layers is caused by the spontaneous emission of photons, which depends on the product of the electron and hole occupation probability in each state; in the bulk carrier, loss is due to both spontaneous photon emission and Shockley-Read-Hall recombination.

The QD parameters used in the simulations are summarized in Table I, whereas the standard material parameters are used for the GaAs, InGaAs, and InAlGaAs layers. Transport across the heterojunctions is modelled according to a graded material approximation.[49]

We show in Figure 7(a) the calculated band diagram in thermal equilibrium and in Figure 7(b) the band diagram with a forward bias of 1 V corresponding to a current density of 124 A/cm^2. The results in Figure 7(b) show a quasi-equilibrium condition, maintained by the thermal coupling among the QD layer states (GS, ES, and WL) and surrounding bulk states. This is confirmed by several experimental results[50,51] at RT and forward bias, where the quasi-thermal distribution is, in general, observed down to about 200 K. For the structure analyzed in this paper, this quasi-equilibrium condition is broken in the two layers next to the p-side, as the electric field sweeps out the bulk electrons, whereas the QD electrons, being well confined in the QDs, are still accumulated in the GS and ES. After calculating the carrier distribution of the various layers, we were then able to simulate the EL spectra, starting from the calculation of the spontaneous emission rate. This analysis is carried on relying on the rate equation model used to represent the carrier dynamics. Although a random population model would be more appropriate to calculate the spontaneous emission rate at any temperature,[51] results in Ref. 51 show

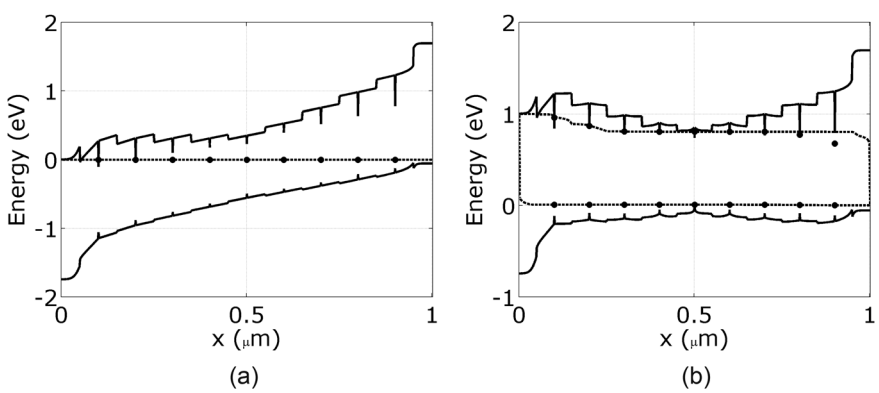

FIG. 7. Room temperature energy band diagrams of the p-i-n junction (in reverse order) embedding structure (B) in the intrinsic layer: (a) under thermal equilibrium; (b) under forward bias of 1 V. The quasi-Fermi levels of electrons and holes are indicated with dashed lines for the bulk and with circles for the QD GS.

that the rate equation model is a good approximation at RT. The spectrum of the spontaneous emission rate reads as[52]

$$R_{sp}(\hbar\omega) = \sum_i C_{sp} \int L(\hbar\omega - \varepsilon) \cdot \rho_i^{e,GS}(\varepsilon_i^{e,GS}) \cdot \rho_i^{h,GS}(\varepsilon_i^{h,GS}) \cdot G_i(\varepsilon_i^{e,GS}) d\varepsilon, \quad (4)$$

where the sum is carried over the QD layers, C_{sp} is a constant that includes the transition matrix elements and the density of the optical mode; the integral accounts for the interplay between the homogeneous broadening linewidth ($L(\hbar\omega)$) and the inhomogeneous broadening due to the size inhomogeneity of the QDs in each layer. $\rho_i^{e,GS}(\varepsilon_i^{e,GS})$ and $\rho_i^{h,GS}(\varepsilon_i^{h,GS})$ are the occupation probabilities of the GS electron and hole state, and the GS recombination energy is $\varepsilon = \varepsilon_i^{e,GS} + \varepsilon_i^{h,GS}$. By analysing with TiberCAD software on the variation of $\varepsilon_i^{e,GS}$ and $\varepsilon_i^{h,GS}$ due to the QD size fluctuations, we have verified that the variation of $\varepsilon_i^{e,GS}$ is responsible for more than 90% of the inhomogeneous broadening of the recombination energy. For this reason, in Eq. (4), we include only the inhomogeneous fluctuations of the GS electron energy and we neglect the hole ones. G is a Gaussian function that reads as

$$G_i\left(\varepsilon_i^{e,GS}\right) = \frac{1}{2\pi\sigma_i^2} e^{-\frac{\left(\varepsilon_i^{e,GS} - \overline{\varepsilon_i^{e,GS}}\right)^2}{\sigma_i^2}}, \quad (5)$$

where $\overline{\varepsilon_i^{e,GS}}$ is the average GS energy of the electrons in the *i-th* layer. $L(\hbar\omega)$ is a Lorentzian function with FWHM equal to 10 meV.

Figure 8 shows the EL spectra calculated according to Eq. (4), with a unitary C_{sp} coefficient. For each layer, we assumed a Gaussian inhomogeneous broadening with FWHM (from left side to central layers of Fig. 7) of 50 meV (x = 0), 60 meV (x = 0.10), 100 meV (x = 0.20), 130 meV (x = 0.30), and 130 meV (x = 0.40). Such values correspond to those reported for RT PL emission spectra of QD metamorphic structures.[24,47,53] As no experimental values are available for the InAs QDs grown on metamorphic InAlGaAs, for the layers on the right side, we assumed a symmetric distribution of the inhomogeneous broadening.

We plot in Figure 8 the EL spectra due to GS emission at an increasing current injection; a FWHM bandwidth of about 400 nm is achieved at J = 1200 A/cm^2. For this case, we also show in dashed lines the contribution of the various layers: the central layers (with peak emissions at 1.6 and 1.42 μm) are those most favoured by carrier filling and therefore give the largest contribution to the spectrum. Despite the lower filling of holes (see Fig. 9), the layers with emissions between 1.29 μm and 1.39 μm contribute to the short wavelength side, thanks to the overlap of their emission lines. The first GaAs layer on the left side (peak emission at 1.2 μm) should contribute to a further extension of the bandwidth, but it suffers of a very poor filling of holes (see Fig. 9): the holes, being injected from the opposite side, are indeed almost completely captured by the lower energy gap layers in the centre. To better investigate the non-uniform distribution of carriers in the various layers, we plot the carrier occupation $\rho_{i,GS}^{e}$ and $\rho_{i,GS}^{h}$ in Figure 9. Electrons are more confined in the QDs because of the higher potential barrier (with respect to the shallow barrier of the holes); therefore, at an equilibrium and a very low injection current, the first layer closer to the n-side is already saturated by electrons, whereas the other layers are almost empty. With the increase in current, all the layers begin to be filled, with predominant electron capture in the central layers. At a high injection current, the GS of most of layers is uniformly filled by electrons with a consequent small electron accumulation in the barrier. On the contrary, the holes, once injected from the p-side, are captured in the first QD layers, but they can also re-escape fast (faster than electrons due to the shallow hole potential); they are transported towards the centre of the junction where they tend to accumulate because of the lower energy gap of the bulk material in the centre. For this reason, the central layers are efficiently filled by holes, whereas the external layers (toward both p- and n-side) are almost empty even at the high injection current. Such a very non-uniform distribution of holes could be mitigated by the use of

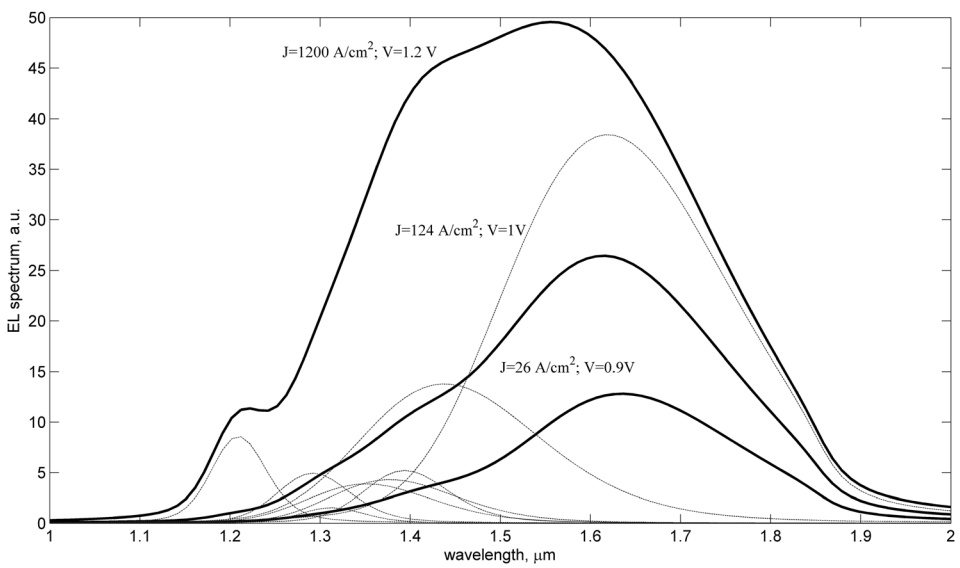

FIG. 8. EL spectrum at different injection conditions. Dashed lines show the contribution of each QD metamorphic layer for the 1.2 V biasing condition.

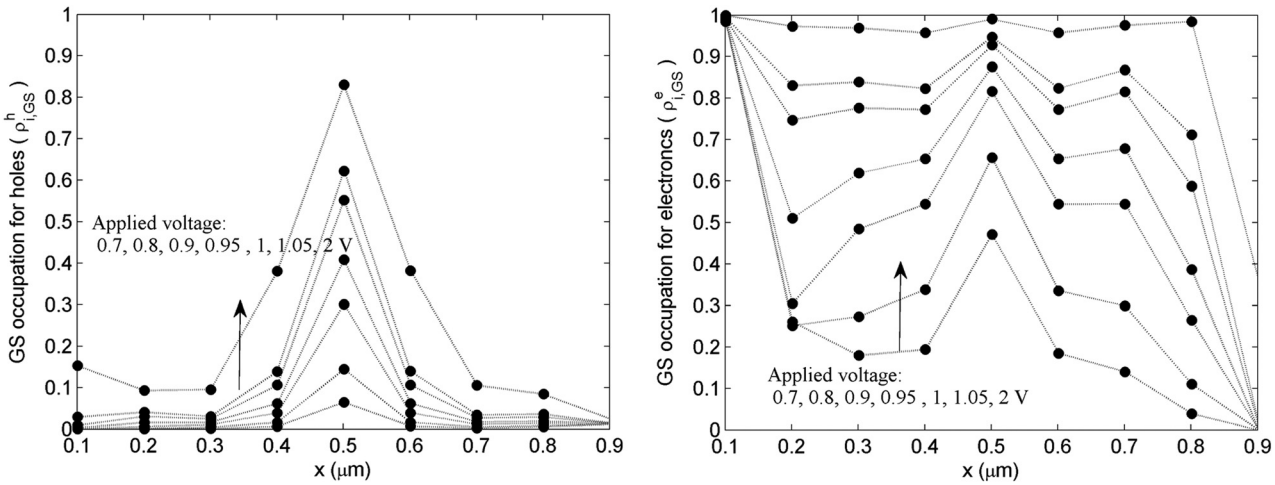

FIG. 9. Ground state occupation probability of holes (left) and electrons (right) in the various QD layers increasing bias voltage; the QD layer position on the x-axis is the same as in Fig. 7. The dashed lines are guide to the eye.

modulation doping of some of the QD layers[54] closer to the n- and p- contacts, and it is now under investigation.

IV. DISCUSSION AND CONCLUSIONS

In this work, we have demonstrated that the metamorphic approach allows us to use two independent parameters (x and y) to finely tune the QD emission energy and intensity, providing design tools to control wavelengths and bandwidth of emission at RT.

It should be noticed here that the possibility of extending the emission to long wavelengths is a peculiar advantage of the metamorphic QDs, as other approaches do not allow such a wide tuning range for structures grown on GaAs.[55,56] In real structures, the emission efficiencies might be different for each layer due to the extrinsic parameters such as the QD density and the presence of structural defects. Such effects have already been studied and methods to compensate for differences in the emission intensity have been put forward such as: (i) techniques to control and spatially confine MB-related defects,[18,57] (ii) multiple stacks of QDs for layers with lower efficiencies, and (iii) more complex grading profiles allowing for a better control of linear defect spatial confinement.[34]

We foresee that even more advanced engineering possibilities exist, as many parameters are available such as: (i) the increase of composition x or the use of MB with different materials to extend wavelength of operation: QDs grown on $In_xGa_{1-x}As$ buffers with $x > 0.40$ have already been reported,[10,13,14] as long as on metamorphic buffers based on GaAsSb;[58,59] (ii) different designs of graded buffers are possible to spatially control structural defect;[34,60,61] (iii) change in parameters such as the density and dimensions of QDs could improve the emission efficiencies and/or wavelength tuning.[42,62]

By inserting the InAs QDs into layers of a step-graded metamorphic $In_xGa_{1-x}As$ buffer, it is possible to obtain a semiconductor structure emitting light in the infrared range (1.0–1.7 μm) with a broad spectrum. By using the TiberCAD software, we carried on model calculations of the QD levels considering the realistic material parameters, taking into account the effect of strain on all relevant parameters (the QD-MB lattice mismatch, bandgaps, electron effective masses, and band offsets) and validating the model with the experimental emission energies. The model results agree within 20 meV with the experimental values for all range of In composition x and also for structures with additional $In_yAl_{1-y}As$ barriers, used to increase the carrier confinement in QDs.

The actual potential of the designed metamorphic material for the realization of an electrically pumped broadband light source is analysed by exploiting a 1D drift-diffusion model coupled to a set of phenomenological rate equations describing the QD carrier dynamics. Thus, the predicted QD populations and the associated EL spectrum take into account both the QD energy distribution and the effect of the multiple barrier layers on current flow. By simulating a symmetric energy profile structure, where $In_{0.30}Al_yGa_{0.70-y}As$ layers were added to the $In_xGa_{1-x}As$ ones, we derived an EL emission spectrum that covers the whole 1.3 μm–1.7 μm range with a 400 nm bandwidth at RT.

Hence, considering the success of metamorphic devices for various photonic applications, we foresee that a broadband device based on metamorphic InAs/InGaAs QDs could be developed and good performances could be expected. An additional advantage of this structure design is the fact that it can be grown on GaAs substrates, thus allowing to fabricate devices using a technology that is already well established for the photonic realm.

ACKNOWLEDGMENTS

The work has been partially supported by COST Action "Nanoscale Quantum Optics." M. Gioannini thanks the support of Fondazione CRT under the initiative "La ricerca dei Talenti." The authors thank Dr. Matthias Auf der Maur for useful discussions.

[1]N. Ozaki, K. Takeuchi, S. Ohkouchi, N. Ikeda, Y. Sugimoto, H. Oda, K. Asakawa, and R. A. Hogg, Appl. Phys. Lett. **103**, 051121 (2013).
[2]M. Rossetti, L. Li, A. Markus, A. Fiore, L. Occhi, C. Velez, S. Mikhrin, I. Krestnikov, and A. R. Kovsh, IEEE J. Quantum Electron. **43**, 676 (2007).

[3]S. M. Chen, K. J. Zhou, Z. Y. Zhang, D. T. D. Childs, M. Hugues, A. J. Ramsay, and R. A. Hogg, Appl. Phys. Lett. **100**, 041118 (2012).
[4]S. Chen, M. Tang, Q. Jiang, J. Wu, V. G. Dorogan, M. Benamara, Y. I. Mazur, G. J. Salamo, P. Smowton, A. Seeds, and H. Liu, ACS Photonics **1**, 638 (2014).
[5]N. Ozaki, T. Yasuda, S. Ohkouchi, E. Watanabe, N. Ikeda, Y. Sugimoto, and R. A. Hogg, Jpn. J. Appl. Phys., Part 1 **53**, 04EG10 (2014).
[6]N. Ozaki, K. Takeuchi, S. Ohkouchi, N. Ikeda, Y. Sugimoto, K. Asakawa, and R. A. Hogg, J. Cryst. Growth **323**, 191 (2011).
[7]L. Li, M. Rossetti, and A. Fiore, J. Cryst. Growth **278**, 680 (2005).
[8]S. K. Ray, T. L. Choi, K. M. Groom, B. J. Stevens, H. Liu, M. Hopkinson, and R. A. Hogg, IEEE J. Sel. Top. Quantum Electron. **13**, 1267 (2007).
[9]H. S. Djie, C. E. Dimas, and B. S. Ooi, IEEE Photonics Technol. Lett. **18**, 1747 (2006).
[10]G. Balakrishnan, S. Huang, T. J. Rotter, A. Stintz, L. R. Dawson, K. J. Malloy, H. Xu, and D. L. Huffaker, Appl. Phys. Lett. **84**, 2058 (2004).
[11]N. V. Kryzhanovskaya, A. Y. Gladyschev, S. Blokhin, Y. G. Musikhin, A. E. Zhukov, M. V. Maksimov, N. Zakharov, A. Tsatsul'nikov, N. N. Ledentsov, P. Werner, F. Guffarth, and D. Bimberg, Semiconductors **38**, 833 (2004).
[12]L. Seravalli, M. Minelli, P. Frigeri, S. Franchi, G. Guizzetti, M. Patrini, T. Ciabattoni, and M. Geddo, J. Appl. Phys. **101**, 024313 (2007).
[13]L. Seravalli, P. Frigeri, G. Trevisi, and S. Franchi, Appl. Phys. Lett. **92**, 213104 (2008).
[14]E. S. Semenova, R. Hostein, G. Patriarche, O. Mauguin, L. Largeau, I. Robert-Philip, A. Beveratos, and A. Lemaitre, J. Appl. Phys. **103**, 103533 (2008).
[15]L. Seravalli, G. Trevisi, P. Frigeri, D. Rivas, G. Munoz-Matutano, I. Suarez, B. Alen, J. Canet, and J. P. Martinez-Pastor, Appl. Phys. Lett. **98**, 173112 (2011).
[16]G. Munoz-Matutano, D. Rivas, A. L. Ricchiuti, D. Barrera, C. R. Fernandez-Pousa, J. Martinez-Pastor, L. Seravalli, G. Trevisi, P. Frigeri, and S. Sales, Nanotechnology **25**, 035204 (2014).
[17]Z. Mi, P. Bhattacharya, and J. Yang, Appl. Phys. Lett. **89**, 153109 (2006).
[18]N. N. Ledentsov, V. A. Shchukin, T. Kettler, K. Posilovic, D. Bimberg, L. Y. Karachinskii, A. Y. Gladyschev, M. V. Maksimov, S. V. Novikov, Y. M. Shernyakov, A. E. Zhukov, V. M. Ustinov, and A. R. Kovsh, J. Cryst. Growth **301–302**, 914 (2007).
[19]T. Kettler, L. Y. Karachinskii, N. N. Ledentsov, V. A. Shchukin, G. Fiol, M. Kuntz, A. Lochmann, O. Schulz, L. Reissmann, K. Posilovic, D. Bimberg, S. V. Novikov, Y. M. Shernyakov, N. Y. Gordeev, M. V. Maksimov, N. V. Kryzhanovskaya, A. E. Zhukov, E. S. Semenova, A. P. Vasil Ev, V. M. Ustinov, and A. R. Kovsh, Appl. Phys. Lett. **89**, 041113 (2006).
[20]W. Guter, J. Schoene, S. P. Philipps, M. Steiner, G. Siefer, A. Wekkeli, E. Welser, E. Oliva, A. W. Bett, and F. Dimroth, Appl. Phys. Lett. **94**, 223504 (2009).
[21]S.-G. Ihn, S. J. Jo, and J.-I. Song, Appl. Phys. Lett. **88**, 132108 (2006).
[22]M. Boudrissa, E. Delos, C. Gaquiere, M. Rousseau, Y. Cordiere, D. Theron, and J. C. De Jaeger, IEEE Trans. Electron Devices **48**, 1037 (2001).
[23]J. A. Czaban and D. A. Thompson, Nanotechnology **21**, 134005 (2010).
[24]L. Seravalli, P. Frigeri, L. Nasi, G. Trevisi, and C. Bocchi, J. Appl. Phys. **108**, 064324 (2010).
[25]L. Seravalli, G. Trevisi, and P. Frigeri, CrystEngComm **14**, 1155 (2012).
[26]L. Seravalli, M. Gioannini, F. Cappelluti, F. Sacconi, G. Trevisi, and P. Frigeri, in *Fotonica AEIT Italian Conference on Photonics Technologies* (2015), p. 1.
[27]M. Auf der Maur, G. Penazzi, G. Romano, F. Sacconi, A. Pecchia, and A. Di Carlo, IEEE Trans. Electron Devices **58**, 1425 (2011).
[28]See www.tiberlab.com for TiberCAD software.
[29]M. Gioannini, A. P. Cedola, N. Di Santo, F. Bertazzi, and F. Cappelluti, IEEE J. Photovoltaics **3**, 1271 (2013).
[30]A. P. Cedola, M. Gioannini, and F. Cappelluti, IET Optoelectron. **9**, 69 (2015).
[31]K. Ludge and E. Schöll, IEEE J. Quantum Electron. **45**, 1396 (2009).
[32]M. Loeser and B. Witzigmann, IEEE J. Quantum Electron. **44**, 505 (2008).
[33]S. Haggett, M. Krakowski, I. Montrosset, and M. A. Cataluna, Opt. Express **22**, 22854 (2014).
[34]F. Romanato, E. Napolitani, A. Carnera, A. Drigo, L. Lazzarini, G. Salviati, C. Ferrari, A. Bosacchi, and S. Franchi, J. Appl. Phys. **86**, 4748 (1999).
[35]F. Capotondi, G. Biasiol, D. Ercolani, V. Grillo, E. Carlino, F. Romanato, and L. Sorba, Thin Solid Films **484**, 400 (2005).
[36]L. Seravalli, C. Bocchi, G. Trevisi, and P. Frigeri, J. Appl. Phys. **108**, 114313 (2010).
[37]D. Barettin, R. De Angelis, P. Prosposito, M. Auf Der Maur, M. Casalboni, and A. Pecchia, Nanotechnology **25**, 195201 (2014).
[38]F. Sacconi, M. Auf der Maur, and A. Di Carlo, IEEE Trans. Electron Devices **59**, 2979 (2012).
[39]M. Povolotskyi and A. Di Carlo, J. Appl. Phys. **100**, 063514 (2006).
[40]L. Seravalli, G. Trevisi, and P. Frigeri, J. Appl. Phys. **114**, 184309 (2013).
[41]H. Jiang and J. Singh, Phys. Rev. B **56**, 4696 (1997).
[42]O. Stier, M. Grundmann, and D. Bimberg, Phys. Rev. B **59**, 5688 (1999).
[43]L. Wang, J. Kim, and A. Zunger, Phys. Rev. B **59**, 5678 (1999).
[44]M. Yahyaoui, K. Sellami, K. Boujdaria, M. Chamarro, and C. Testelin, Semicond. Sci. Technol. **28**, 125018 (2013).
[45]I. Vurgaftman, J. Meyer, and L. Ram-Mohan, J. Appl. Phys. **89**, 5815 (2001).
[46]L. Seravalli, G. Trevisi, P. Frigeri, S. Franchi, M. Geddo, and G. Guizzetti, Nanotechnology **20**, 275703 (2009).
[47]L. Seravalli, P. Frigeri, M. Minelli, P. Allegri, V. Avanzini, and S. Franchi, Appl. Phys. Lett. **87**, 063101 (2005).
[48]T. R. Nielsen, P. Gartner, and F. Jahnke, Phys. Rev. B **69**, 235314 (2004).
[49]A. H. Marshak and K. M. van Vliet, Solid-State Electron. **21**, 417 (1978).
[50]P. Spencer, E. Clarke, R. Murray, K. M. Groom, R. R. Alexander, and R. A. Hogg, Phys. Rev. B **83**, 205407 (2011).
[51]I. O'Driscoll, P. Blood, and P. M. Smowton, IEEE J. Quantum Electron. **46**, 525 (2010).
[52]M. Gioannini, IEEE J. Quantum Electron. **40**, 364 (2004).
[53]L. Seravalli, G. Trevisi, P. Frigeri, R. J. Royce, and D. J. Mowbray, J. Appl. Phys. **112**, 034309 (2012).
[54]M. Rossetti, L. Li, A. Fiore, L. Occhi, C. Velez, S. Mikhrin, and A. Kovsh, IEEE Photonics. Technol. Lett. **18**, 1946 (2006).
[55]D. Guimard, S. Tsukamoto, M. Nishioka, and Y. Arakawa, Appl. Phys. Lett. **89**, 083116 (2006).
[56]O. Schumann, S. Birner, M. Baudach, L. Geelhaar, H. Eisele, L. Ivanova, R. Timm, A. Lenz, and S. Becker, Phys. Rev. B **71**, 245316 (2005).
[57]Z. Mi, J. Yang, and P. Bhattacharya, J. Cryst. Growth **301–302**, 923 (2007).
[58]H. Liu, Y. Qiu, C. Y. Jin, T. Walther, and A. G. Cullis, Appl. Phys. Lett. **92**, 111906 (2008).
[59]Y. Xin, L. Vaughn, L. R. Dawson, A. Stintz, Y. Lin, L. F. Lester, and D. L. Huffaker, J. Appl. Phys. **94**, 2133 (2003).
[60]R. Jakomin, M. de Kersauson, M. El Kurdi, L. Largeau, O. Mauguin, G. Beaudoin, S. Sauvage, R. Ossikovski, G. Ndong, M. Chaigneau, I. Sagnes, and P. Boucaud, Appl. Phys. Lett. **98**, 091901 (2011).
[61]F. Gao and G. Li, Appl. Phys. Lett. **104**, 042104 (2014).
[62]P. B. Joyce, T. J. Krzyzewski, G. R. Bell, T. S. Jones, S. Malik, D. Childs, and R. Murray, Phys. Rev. B **62**, 10891 (2000).